Partial Internal Wetting of Catalyst Particles: Hysteresis Effects

D. N. Jaguste and S. K. Bhatia
Dept. of Chemical Engineering, Indian Institute of Technology, Powai, Bombay 400 076, India

Condensation-evaporation hysteresis associated with the internal wetting of catalyst particles is examined here by the Kelvin and Cohan equations. It is shown that in the absence of information on the thermal history, it is difficult to predict the extent of internal wetting and the associated reaction rate, for states with partial internal wetting, with the actual rate lying anywhere between the limits specified by the Kelvin and Cohan equations. Hysteresis effects arising from thermal cycling are discussed, and the predictions are shown to agree with the experimental data of Kim and Kim (1981a). Experimentally observed transitions between states with markedly different extents of internal wetting and with associated sudden evaporation or condensation are also rationalized by the theory.

Introduction

The phenomenon of partial internal wetting of catalyst particles remains one of the less-understood features of three phase systems, although it is of immediate concern in the analysis of trickle-bed reactors. This is the case despite several experimental studies reporting the existence of partial internal wetting and associated hysteresis effects (Sedriks and Kenney, 1973; Satterfield and Ozel, 1973; Hanika et al., 1975, 1976; Kim and Kim, 1981a,b). Unusual and complex behavior arising from vapor-liquid transition in trickle beds has also been observed by various investigators (Hanika et al., 1975, 1976; Satterfield and Way, 1972; Germain et al., 1974; Eigenberger and Wegerle, 1982; Tukac et al., 1986), making it all the more imperative that the physical processes affecting such systems be more thoroughly examined.

Recently, some efforts have been made in the above direction (Bhatia, 1988, 1989; Harold, 1988a), in which the interplay between capillary condensation phenomena and thermal effects has been examined and the resulting effect on multiplicity and effectiveness factor elucidated. These works have highlighted the applicability of the Kelvin equation of capillary thermodynamics in predicting the degree of internal wetting, a parameter used as an independent variable in prior analyses (Sakornwimon and Sylvester, 1982; Martinez et al., 1981), or arbitrarily assumed to be unity (Ramchandran and Smith, 1979; Mills and Dudukovic, 1980, 1982; Herskowitz, 1981a,b; Yentekakis and Vayenas, 1987; Harold, 1988b; Tan, 1988). An important conclusion in the studies of Bhatia and of Harold is that the extent of internal wetting has a sensitive dependence on thermal effects and strongly influences the effectiveness factor because of the dependence of transport rates on this variable. In addition, the interplay between capillary condensation phenomena and thermal effects is found to give rise to multiplicity of degree of liquid filling and effectiveness factors. Although this multiplicity can give rise to some hysteresis effects, a feature not explored in these works is the hysteresis arising from the differences between condensation and evaporation equilibria in the pores. While the evaporation occurring with temperature increase resulting from a change in process variables follows the Kelvin equation, the condensation occurring with temperature reduction follows the Cohan equation (Bhatia, 1988). This can lead to additional hysteresis effects not anticipated in these prior analyses.

This study attempts to reconcile the ideas contained in the works of Bhatia (1988, 1989) with experimental findings. The possibility of hysteresis is examined by means of the Kelvin and Cohan equations, and the importance of thermal history in establishing the current state of a catalyst particle is discussed. The analysis is applied to the data of Kim and Kim (1981a) on the hydrogenation of cyclohexene, and it is shown that the experimentally observed, but previously unexplained, hysteresis can be rationalized by this approach.

Mathematical Model

In this work, we consider the reaction $aA + bB \rightarrow cC$, in which A and C are condensable while B is not. Further, it is considered

that the reaction rate is zero order with respect to the concentration of A, both in the liquid and vapor phases. Several systems have rate behavior consistent with this assumption, notable among these being the hydrogenation of cyclohexene, in which the rate is independent of cyclohexene concentration (Madon et al., 1978; Segal et al., 1978). Since A and C are condensable, some internal liquid filling can occur because of capillary condensation in the micropores. The segregated liquid pockets thus formed would hinder the gas-phase transport reducing the effective diffusivity. To study the associated transition and reaction effects, we consider a mathematical model similar to Bhatia's (1989), for spherical catalyst pellets surrounded by gaseous reactant B saturated with condensable A, and containing noncondensable inserts I, as follows.

Mass transfer

Mass transfer is considered to be governed by vapor-phase transport, yielding:

$$\frac{1}{\eta^2}\frac{d}{d\eta}\left[\eta^2 D^*_{eA}\frac{dy_A}{d\eta}\right]=\theta\phi^2(\theta)y_B^m \tag{1}$$

$$\frac{1}{\eta^2}\frac{d}{d\eta}\left[\eta^2 D^*_{eB}\frac{dy_B}{d\eta}\right]=\frac{b}{a}\theta\phi^2(\theta)y_B^m \tag{2}$$

$$\frac{1}{\eta^2}\frac{d}{d\eta}\left[\eta^2 D^*_{eC}\frac{dy_C}{d\eta}\right]=-\frac{c}{a}\theta\phi^2(\theta)y_B^m \tag{3}$$

in which the pressure variation is neglected, and any bulk flow contribution arising due to reaction is included in the diffusivity term of the respective equation. Here, the overall kinetics:

$$\hat{R}_A=k(T)P_T^m y_B^m \tag{4}$$

has been assumed, accounting for both liquid-filled and vapor-filled regions. In the presence of local vapor-liquid equilibrium, the vapor- and liquid-filled regions must have the same specific rate if surface reaction controls, as explained earlier (Bhatia, 1988, 1989). However, the two rates may differ, when adsorption is not rapid or when vapor-liquid equilibrium is not present. Equations 2 and 3 may be combined with Eq. 1 along with the symmetry condition at $\eta=0$ to yield:

$$D^*_{eB}\frac{dy_B}{d\eta}=\frac{b}{a}D^*_{eA}\frac{dy_A}{d\eta} \tag{5}$$

$$D^*_{eC}\frac{dy_C}{d\eta}=-\frac{c}{a}D^*_{eA}\frac{dy_A}{d\eta} \tag{6}$$

which may then be used to replace Eqs. 2 and 3, respectively. We consider the case of high Thile modulus, since as pointed out by Bhatia (1988), this situation is more likely to result in multiplicity of extent of internal wetting. Under this condition, the concentration and flux of the limiting reactant, assumed to be the condensable A, will become zero at some position η_c, providing the boundary conditions:

$$y_A(\eta_C)=\frac{dy_A}{d\eta}(\eta_C)=0 \tag{7}$$

Further, neglecting the external mass transfer resistance:

$$\begin{aligned} y_A(1)&=y_A^o\\ y_B(1)&=y_B^o\\ y_C(1)&=y_C^o \end{aligned} \tag{8}$$

In Eqs. 1, 2 and 3, the Thile modulus is given by:

$$\phi=R_o\left[\frac{qk(T)P_T^m\tau_v}{\epsilon D^o_{AC}C_T^o}\right]^{1/2} \tag{9}$$

where ϵ is the total porosity, and τ_v the tortuosity of the totally vapor-filled catalyst. We consider the case where the tortuosity varies with the extent of liquid filling, so that

$$D^*_{eA}(\eta)=\frac{1}{\epsilon\tau^*}\int_{\rho_C(\eta)}^{\infty}D^*_{Am}(\rho)f(\rho)d\rho \tag{10}$$

$$D^*_{eB}(\eta)=\frac{1}{\epsilon\tau^*}\int_{\rho_C(\eta)}^{\infty}D^*_{Bm}(\rho)f(\rho)d\rho \tag{11}$$

$$D^*_{eC}(\eta)=\frac{1}{\epsilon\tau^*}\int_{\rho_C(\eta)}^{\infty}D^*_{Cm}(\rho)f(\rho)d\rho \tag{12}$$

in which ρ_C is the critical dimensionless pore radius, below which liquid filling occurs, and where it is assumed

$$\tau^*=\frac{\tau}{\tau v}=1+\beta\epsilon_L \tag{13}$$

as one would expect the tortuosity to increase with ϵ_L, the fractional liquid filling, given by:

$$\epsilon_L=\int_0^{\rho_C}f(\rho)d\rho \tag{14}$$

where

$$f(\rho)=\frac{d\epsilon}{d\rho} \tag{15}$$

is the pore volume distribution. In Eqs. 10, 11 and 12, the dimensionless mixture diffusivities, which include bulk flow under isobaric conditions, are expressed as in Bhatia (1989) as:

$$D^*_{Am}=\left[\frac{d_{AB}}{\theta^{1.75}}\left(y_B-\frac{b}{a}y_A\right)+\frac{1}{\theta^{1.75}}\left(y_C+\frac{c}{a}y_A\right)+\frac{d_{AI}}{\theta^{1.75}}y_I+\frac{d_{AK}}{\theta^{0.5}\rho}\right]^{-1} \tag{16}$$

$$D^*_{Bm}=\left[\frac{d_{AB}}{\theta^{1.75}}\left(y_A-\frac{a}{b}y_B\right)+\frac{d_{BC}}{\theta^{1.75}}\left(y_C+\frac{c}{b}y_B\right)+\frac{d_{BI}}{\theta^{1.75}}y_I+\frac{d_{BK}}{\theta^{0.5}\rho}\right]^{-1} \tag{17}$$

$$D^*_{Cm}=\left[\frac{1}{\theta^{1.75}}\left(y_A+\frac{a}{c}y_C\right)+\frac{d_{BC}}{\theta^{1.75}}\left(y_B+\frac{b}{c}y_C\right)+\frac{d_{CI}}{\theta^{1.75}}y_I+\frac{d_{CK}}{\theta^{0.5}\rho}\right]^{-1} \quad (18)$$

In Eq. 13, β is a constant parameter. This linear dependence of tortuosity on liquid filling is clearly an approximation. The effect of liquid filling on tortuosity may be more accurately captured by means of percolation and effective medium concepts (Kirpatrick, 1971, 1973); however, for this discussion the linear approximation is used.

Vapor-liquid equilibrium

Following the earlier derivation (Bhatia, 1988), vapor-liquid equilibrium across a curved interface is given by:

$$\frac{y_i P_T}{x_i P_i^o}=\exp\left[-\frac{2\sigma\bar{v}_i}{R_g T r_m}\right]$$

where

$$\frac{2}{r_m}=\left[\frac{1}{r_1}+\frac{1}{r_2}\right]$$

Here r_m is the mean radius of curvature of the interface, and r_1, r_2 are the two principal radii of the curved interface, as defined in the pure-component form of the above equation given by Gregg and Sing (1967). By convention, a radius of curvature is given a positive sign when its center of curvature lies on the vapor side of the interface.

During capillary condensation in a cylindrical pore, the vapor-liquid interface is known to pass through a series of unstable configurations before the final stable hemispherical shape is attained. However, at the two extreme situations, namely, evaporation of liquid from a liquid-filled pore and inception of condensation in a vapor-filled pore, the meniscus takes hemispherical and cylindrical shapes, respectively (Everett and Haynes, 1972). The mean radius of curvature r_m for these two cases is readily related to the radius (r) of the cylindrical pore. Thus, for a cylindrical meniscus, for which $r_1=r$ and $r_2=\infty$ one obtains $r_m=2r$. For a hemispherical-shaped meniscus, r_m can be related to r by:

$$r_m=\frac{r}{\cos\theta_c}$$

where θ_c is the contact angle, which may differ from the equilibrium property $\hat{\theta}$. Consequently, for the perfect hemisphere, for which $\theta_c=0$ and $r_1=r_2=r$, one obtains $r_m=r$. Thus, although the vapor-liquid equilibrium in a porous body is uniquely defined with respect to the curvature of the meniscus, it is not so with respect to the pore radius. However, the condition for the inception of condensation in a vapor-filled pore and that for evaporation in a liquid-filled pore could be given by the modified Cohan and Kelvin equations (Bhatia, 1988), which are the special cases of the above more general result, which applies to any shape of vapor-liquid interface having constant curvature.

Assuming that B and I are noncondensable, the vapor-liquid equilibrium for evaporation in the presence of a hemispherical meniscus is given by (Bhatia, 1988, 1989):

$$\frac{y_A}{P_A^{o*}(\theta)}\exp(\alpha/\rho_c\theta)+\frac{y_c}{P_c^{o*}(\theta)}\exp(\alpha h_c/\rho_c\theta)=1 \quad (19)$$

while for condensing vapor with a cylindrical meniscus (Bhatia, 1988)

$$\frac{y_A}{P_A^{o*}(\theta)}\exp(\alpha/2\rho_c\theta)+\frac{y_c}{P_c^{o*}(\theta)}\exp(\alpha h_c/2\rho_c\theta)=1 \quad (20)$$

in which we have taken the contact angle to be 0 and assumed α to be independent of temperature. As before, we assume:

$$P_A^{o*}(\theta)=P^*_{AO}\exp[-\Delta H^*_A(1-\theta)/\theta] \quad (21)$$

$$P_C^{o*}(\theta)=P^*_{CO}\exp[-\Delta H^*_C(1-\theta)/\theta] \quad (22)$$

Heat transfer

As before, the pellet has been assumed internally isothermal, but with external heat transfer resistance, yielding:

$$\theta-1=\psi\frac{D^*_{eA}(1)}{\theta}\left[\frac{dy_A}{d\eta}\right]_{\eta=1} \quad (23)$$

Results and Discussion

Model parameters

To investigate the hysteresis effects predicted by the above model, parameter values were chosen to represent the cyclohexene hydrogenation reaction at 295 K, whose hysteresis data appeared in the literature (Kim and Kim, 1981a). These authors reported the transitions and hysteresis effects obtained on varying the bulk mole fraction of hydrogen in two similar catalysts, but of different activity, and it is the purpose of this study to reconcile the above model with their findings. Consequently, the model parameter values were chosen to be consistent with the conditions of their experiments. Since the model equations are based on the assumption of isobaric conditions, a theoretical demonstration of the validity of this assumption, for the experimental conditions of Kim and Kim, is provided in the Appendix. Table 1 provides the values of the physical properties that were used in estimating the model parameters

Table 1. Physical Properties of A, B, C and I at 295 K

Property	A C_6H_{10}	B H_2	C C_6H_{12}	I N_2
Vapor pres., kPa	10.27	—	11.33	—
Latent heat, MJ/kmol	30.48	—	29.98	—
Liquid molar vol., m^3/kmol	0.105	—	0.108	—
Surface tension, N/m	0.0253	—	0.0253	—
Bulk diff. in $A\times10^4$, m^2/s	—	0.335	0.0268	0.08
Bulk diff. in $B\times10^4$, m^2/s	0.335	—	0.332	0.772
Bulk diff. in $I\times10^4$, m^2/s	0.08	0.772	0.079	—
Knudsen diff. in 36 A radius pore 10^7, m^2/s	6.62	42.4	6.54	11.3

Table 2. Catalyst Pellet Properties

Property	Value
Size 10^3, m	4.6 dia. 4.8 long
Weight 10^3, kg	0.1157
Density 10^{-3}, kg/m^3	1.45
Microporosity	0.528
Macroporosity	0.0878
Mean micropore radius, Å	36
Mean macropore radius, Å	1,460

with A taken as cyclohexene, B as hydrogen, C as cyclohexane, and I as nitrogen. The heat of reaction was taken as 117 MJ/kmol. The properties of their catalyst pellets are given in Table 2. Table 3 lists the values of the dimensionless model parameters obtained based on the properties given in Tables 1 and 2. Except for the tortuosity parameter β in Table 3, all other parameters are known independent of the data, being physical- or chemical-property-related. The pore-size distribution of their pellet was also reported by Kim and Kim and is plotted in dimensionless form in Figure 1, with different segments being linearized on the coordinates used.

The kinetics of the hydrogen cyclohexene reaction have been studied in the literature by various investigators, and here we have used the results of Lee (1980) for the vapor-phase reaction reported by Kim and Kim (1981b) as:

$$\text{Rate (kmol/m}^3\text{ cat}\cdot\text{s)} = k\,P_{H_2}^m \tag{24}$$

For $T<313$ K:

$$k = 1.06\times10^{14}\times(0.133)^{-m}\exp[-21{,}400/R_gT]$$

$$m = 5.23 - 0.0151\,T \tag{25}$$

For $T>313$ K:

$$k = 133{,}537\exp[-7{,}930/R_gT]$$

$$m = 0.5 \tag{26}$$

in which P_{H_2} is specified in kPa. For completely liquid-filled catalyst, Madon et al. (1978) report a first-order dependency on partial pressure and provide $k = 1{,}654.13\times\exp(-6{,}760/R_gT)$, $m=1$ for their data, with rates lower (by a factor of 2 or more) than the values obtained from the above constants

Table 3. Dimensionless Model Parameters

Parameter	Value	Parameter	Value
a	1	ΔH_A^*	12.34
b	1	ΔH_C^*	12.13
c	1	P_{Ao}^*	0.101
d_{AB}	0.08	P_{Co}^*	0.111
d_{AI}	0.34	y_A^o	0.101
d_{AK}	4.048	y_C^o	0.0
d_{BC}	0.081	α	0.6
d_{BI}	0.035	h_c	1.03
d_{BK}	0.632	ϵ	0.6158
d_{CI}	0.34	ϕ_o	22.71 (low) 28.41 (medium)
d_{CK}	4.097	β	1.24

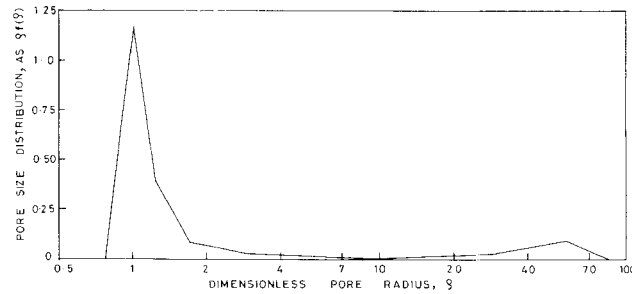

Figure 1. Pore-size distribution of pellets used by Kim and Kim (1981a) in dimensionless coordinates as a plot of $\rho f(\rho)$ vs. ρ.

for the vapor-filled catalyst rates, indicating the possibility of adsorption proceeding at rates comparable to surface reaction in one or both of the cases. The above activation energy for the liquid phase and for the vapor phase in Eqs. 25 and 26 suggests that adsorption effects are significant in the liquid phase, while surface reaction controls for the vapor phase below 313 K [the region in which the data of Kim and Kim lie, as indicated by Kim (1989)]. The former conclusion is supported by the results of Madon et al. (1978). However, it is also not clear if vapor-liquid equilibrium existed in the conditions of Madon et al., as their catalyst was completely liquid-filled.

In calculating the Thiele modulus, which varies with temperature, a constant parameter ϕ_o was defined so that

$$\phi = \phi_o\left[\frac{k(T)P_T^m}{k_o}\right]^{1/2} \tag{27}$$

where k_o represents the value of kP_T^m for the vapor-filled catalyst at 295 K. The value of ϕ_o is based on a value of τv, the tortuosity of the vapor-filled catalyst, of 4.0 and a value of q, the catalyst activity parameter for the corresponding catalyst, obtained from Kim and Kim (1981b). The value of β was chosen for matching the rate data, as discussed in a subsequent section.

Extent of liquid filling

The extent of liquid filling of the pore structure has an important influence on the reaction rate because transport rates, being largely determined by vapor diffusion, are hindered by the presence of the dispersed liquid phase. An interesting feature of the liquid filling, however, is that the vapor-liquid equilibrium condition is not uniquely defined with respect to pore radius but is bounded by the Kelvin and Cohan equations given in Eqs. 19 and 20, respectively. Between the limits specified by these equations at a given temperature, a range of critical pore radii, below which liquid filling occurs, is possible, and imposed changes in temperature will only change the curvature of menisci in the existing liquid-filled pores without leading to appreciable condensation or evaporation till the appropriate limiting relation is satisfied. When this occurs, the entire volume contained in the pores having critical size is filled or emptied. Thus, the current state of liquid filling of the particle at any time depends on the history, and one can anticipate hysteresis effects.

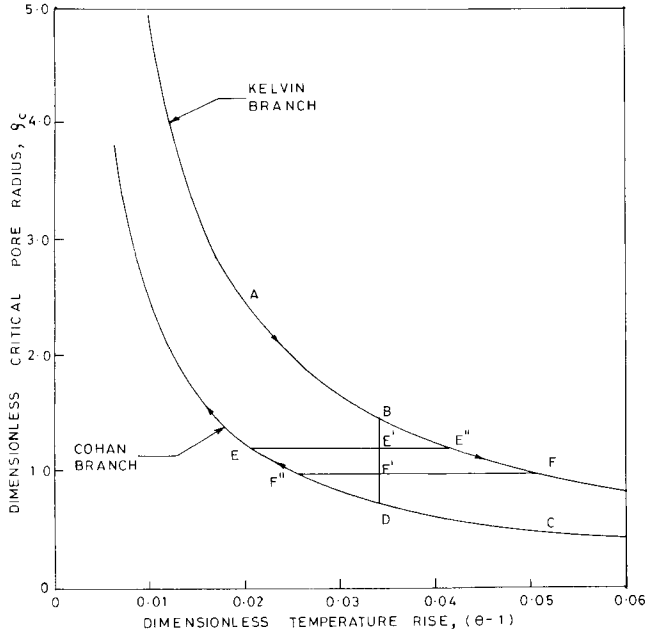

Figure 2. Variation of dimensionless critical pore radius below which liquid filling occurs, with dimensionless temperature rise at $T_o = 295$ K.

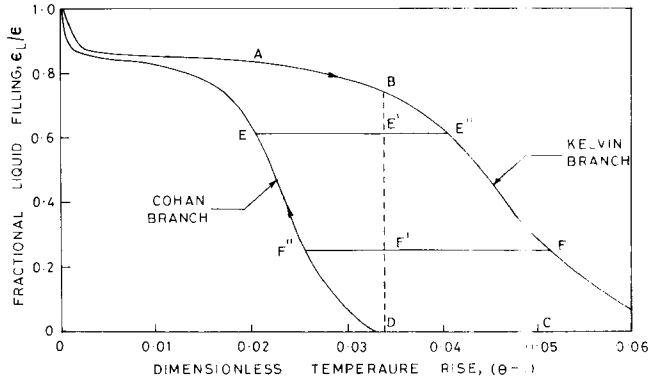

Figure 3. Variation of fractional liquid filling of pores, with dimensionless temperature rise at $T_o = 295$ K.

To investigate this, we consider the solutions to Eqs. 19 and 20 depicted on a plot of ρ_c vs. $(\theta - 1)$, as in Figure 2. This figure is based on the ambient values of y_A and y_C and other parameters specified in Table 3 and applies to the surface of the catalyst pellet. However, it holds very well even in the interior of the pellet because of the similarity of the properties of A and C (cyclohexene and cyclohexane, respectively) in Table 1, and the relatively large diffusivity of B (hydrogen) leading to only a small gradient in its mole fraction.

As seen in Figure 2, a range of pore radii, below which liquid filling occurs, is possible at any pellet temperature θ. Thus, at a temperature rise of $(\theta - 1) = 0.034$, the critical pore radius can lie anywhere between 0.72 and 1.44, so that history effects are important. Consider, for example, the temperature increase of a pellet originally at $A(\rho_c = 2.42,\ \theta - 1 = 0.02)$ which may occur due to change in the external flow rate or bulk mole fraction of B. The critical pore radius will follow the Kelvin curve and at point B it will be reduced to 1.44 whence the temperature rise is 0.034.

On the other hand, on heating from point $E(\rho_c = 1.19,\ \theta - 1 = 0.02)$, which has the same temperature as A, evaporation from pores smaller than $\rho = 1.19$ will not occur until the pellet reaches E'' where the temperature rise is 0.041. Therefore, in this case, $\rho_c = 1.19$ at the temperature rise of 0.034 (point E' on path EE''). Similarly, on cooling from a point such as C with the temperature rise of 0.051, the Cohan branch is followed and at a temperature rise of 0.034 the critical pore radius is 0.72 (point D on path CD), whereas on cooling from point $F(\rho_c = 0.97,\ \theta - 1 = 0.051)$ further condensation does not occur till the temperature rise has dropped to 0.025 (point F''). So, in this case, at a temperature rise of 0.034 $\rho_c = 0.97$ as at point F' on path FF''. Thus, the dependence of the critical pore radius on the pellet temperature is in the form of a clockwise hysteresis loop (e.g., $EE''FF''E$ in Figure 2).

The variation of the fractional liquid-filled pore volume, corresponding to the results in Figure 2, depends on the pore-size distribution of the pellet. For the pore-size distribution of Figure 1, ϵ_L may be calculated using Eq. 14, and the results are presented in Figure 3. In this case one sees rather large differences in the fractional liquid filling for temperature changes causing only modest changes in the critical pore size in Figure 2, as evidenced by the large difference in the pore filling level (0.61 and 0.25) between the upper and lower branches of hysteresis loop $EE''FF''E$ in Figure 3. Similarly, at a temperature rise of 0.034, the fractional pore filling by liquid varies from a lower level of 0 at D (as the minimum dimensionless pore size is 0.75, as seen in Figure 1, while at D only pores smaller than size 0.72 are liquid-filled) to a value of 75% at B. The actual value of the extent of liquid filling at any time can therefore be anywhere between these values (0 and 75%), depending on the history. Since transport and hence reaction rates are a sensitive function of the extent of pore filling by liquid (Bhatia, 1989), one can anticipate large differences in the reaction rate for pellets with different thermal histories even when exposed to the same ambient condition, and this is discussed below in terms of effectiveness factor hysteresis.

Effectiveness factor

In calculating the degree of pore filling above, only Eqs. 19 and 20 were required for any specified temperature. For estimating effectiveness factors, it is necessary, however, to solve the model equations in Eqs. 1 and 5–23. This was done using the orthogonal collocation method (Finlayson, 1972) for discretizing the space variable, and Gauss-Legendre quadrature for integrals over the pore-size distribution, for the parameter values given in Table 3. The effectiveness factor was expressed as:

$$E = \frac{3}{\phi_o^2 (y_B^o)^{m_o} \theta} \left[D_{eA}^* \frac{dy_A}{d\eta} \right]_{\eta = 1} \tag{28}$$

and represents the ratio of the actual rate to that of the vapor-filled catalyst at bulk conditions.

Kim and Kim (1981a) have provided data on measured reaction rates for cyclohexene hydrogenation for two similar catalysts but of different activity, showing the hysteresis with respect to the variations in bulk mole fraction hydrogen at a

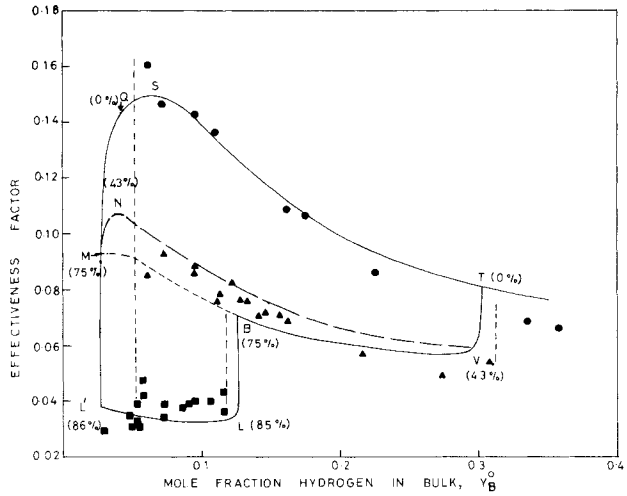

Figure 4. Model predictions vs. experimental data of Kim and Kim (1981a) for effectiveness factor hysteresis with variation in bulk mole fraction hydrogen.

For low activity catalyst ($q = 0.23$) at $T_o = 295$ K. Numbers in parenthesis indicate percent liquid filling of the pore structure.

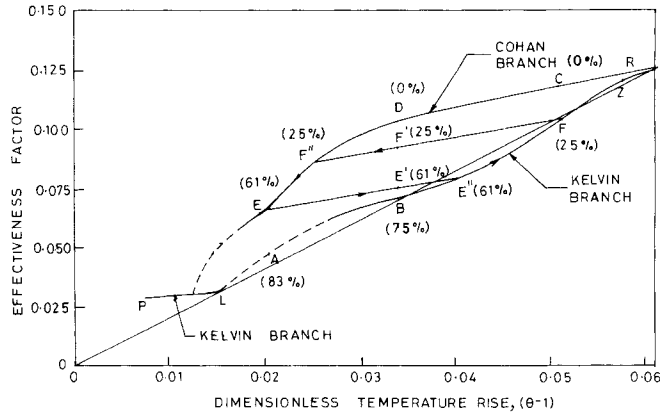

Figure 5. Variation of effectiveness factor with dimensionless temperature rise.

At $P_{H_2} = 12.67$ kPa, $T_o = 295$ K for low activity catalyst ($q = 0.23$). Numbers in parenthesis indicate percent liquid filling of the pore structure.

bulk temperature of 295 K. Since the parameters in Table 3 were chosen to correspond to the conditions of their experiments, direct application to their data was possible. Figure 4 shows the experimental and model-calculated effectiveness factor variation with mole fraction hydrogen for their low activity catalyst, for which they indicated that $q = 0.23$. The solid lines represent the calculated results and the dashed lines correspond to the experimentally observed approximate points of transition which, given the difficulty in measurements, are well represented by the model.

In performing the calculations for Figure 4, an important variable is the heat transfer coefficient imbedded within the parameter ψ. Since the thermal conductivity of hydrogen and nitrogen (the inert) differ vastly, this variable, and hence ψ, are a strong function of bulk composition. In applying the model to the data, it was found that the correlation tried by Kim and Kim (1981a) predicted too high a value of ψ to correspond to the data, and hence the experimental rate data were used to estimate the variation of ψ with respect to the composition. For this purpose, Eqs. 1, 5-22 and 28 were solved to provide the effectiveness factor variation with respect to the temperature as in Figure 5, for a given mole fraction hydrogen. The steady-state effectiveness factor and temperature at that bulk composition were then graphically estimated from the intersection of the branches in Figure 5 with the line:

$$E = \frac{3}{\phi_o^2 (y_B^o)^{m_o} \psi} (\theta - 1) \tag{29}$$

which satisfies Eqs. 23 and 28, with the value of ψ so chosen as to match the experimental and predicted effectiveness factors on all the branches simultaneously as closely as possible. Since as many as three steady states exist at a given bulk composition, this procedure provided a fairly sharp estimate of ψ for all the steady states to be approximated satisfactorily.

To interpret the various branches of Figure 4, we turn first to Figure 5 which shows the variation of effectiveness factor with temperature at a bulk hydrogen partial pressure of 12.67 kPa ($y_B^o = 0.125$). Kelvin branch PL on this figure was obtained on the basis of the rate expression $k = 1{,}654.13 \exp(-6{,}760/R_g T)$ and $m = 1$ corresponding to the values for liquid-filled pores (Madon et al., 1978), and each point on branch $L'L$ of Figure 4 lies on the branch PL for the appropriate value of y_B^o. As seen from Figures 1, 2 and 3, for the temperature range corresponding to branch PL the degree of internal wetting is about 85%, and the critical pore radius lies in the range of 3.2 to 6 so that all the micropores are wetted while the macropores being in the radius range of 10 to 85 are vapor-filled. This was the only way that branch $L'L$ of Figure 4 could be explained and agrees with the prior interpretation of Kim and Kim (1981b).

Branch BFZ on Figure 5 corresponds to the Kelvin branch with the kinetics following the vapor-phase rate expression in Eqs. 24-26, and at point B the internal wetting is 75% with critical pore radius being 1.44. At this point, it is seen that the micropores are beginning to open up to the vapor, so that the vapor-liquid contacting inside the microparticles which comprise the pellet will be considerably enhanced. To obtain the transition from L to B in Figure 4, it was found necessary to assume that when the internal wetting reduces below 85% the applicable rate expression shifts gradually from that for the liquid phase to that for the vapor phase, and before 75% wetting the rate corresponds to that obtained from the vapor-phase expression with vapor-liquid equilibrium. In that case, the line corresponding to Eq. 29 (line LBR) is tangent to the curve PLB at L, producing the transition from L to B.

While the precise reason for the shift in rate expression from the liquid-phase expression to that for the vapor phase requires more direct investigation and cannot be established from the data used, some clue can be obtained from the observation that on branch PL in Figure 5 the microparticles comprising the pellet are essentially liquid-filled. Since in this case the internal surface is almost entirely in the micropores, this situation somewhat parallels that of Madon et al. (1978), who used totally liquid-filled pellets, and the rate therefore corresponds to that of the liquid phase in the absence of any local vapor. However, with reduction in the degree of wetting, some of the micropores open up and, with improved vapor-liquid

contacting due to the presence of sufficient local vapor in the microparticles, the rate appears to become that corresponding to the vapor phase. The specific rates of reaction in the vapor- and liquid-filled pores are then therefore equal. Even though adsorption may not be in equilibrium in the liquid phase, it is possible that with good vapor-liquid contacting, rapid surface diffusion of adsorbed species from the vapor-filled pores may cause the reaction even in the liquid-filled pores to be at the vapor-phase rate. It is very likely that the radically improved vapor-liquid contacting at point L is due to a percolation phenomenon. Thus, with increase in temperature along branch PL at point L, the vapor-filled part of the microparticles crosses the percolation threshold (Mohanty et al., 1982; Wicke and Bartsch, 1990) so that the vapor no longer exists in isolated pockets but forms a continuous interconnected phase pervading the microparticles. However, this is only speculative and other alternative explanations may also be proposed. More direct studies of this aspect are clearly needed.

Branch BV in Figure 4 is obtained from intersection of the line corresponding to Eq. 29 with Kelvin branch BFZ for each bulk composition (branch BFZ in Figure 5 corresponds to $y_B^o = 0.125$). On branch BV the internal wetting reduces from 75% to 43% before transition occurs at V. At this point, the effectiveness factors at T and V were most closely approximated, only when the line corresponding to Eq. 29 was tangent to the branch BFZ for $y_B^o = 0.3$, yielding the transition at V.

Branch RDE in Figure 5 corresponds to the Cohan branch obtained upon condensation, starting with the vapor-filled catalyst, and on varying y_B^o produces branch TSQ in Figure 4. The transition from V to T produces a vapor-filled catalyst, and condensation begins at Q on branch TSQ if y_B^o is reduced. On TS, the vapor-filled portion of branch TSQ, one can move in both directions on changing y_B^o, consistent with the findings of Kim and Kim (1981a). If, however, y_B^o is reduced below the value at Q (0.044), capillary condensation rapidly ensues and beyond 75% liquid filling, as the vapor-liquid contacting in the microparticles becomes poor and the rate expression shifts to that for the liquid phase, a transition to point L' on branch $L'L$ occurs. This is because the line corresponding to Eq. 29 no longer intersects the Cohan branch on the curve corresponding to RDE of Figure 5, for the appropriate bulk composition. This transition is seen in Figure 4 to predict satisfactorily the corresponding transition observed by Kim and Kim (1981a), given the difficulty in observing it precisely because of the extreme sensitivity of the effectiveness factor at this point.

Branch BM on Figure 4 is obtained by reducing the bulk mole fraction of hydrogen (y_B^o), after having undergone transition LB. Since this causes a reduction in temperature, further liquid filling will therefore not occur till the Cohan limit at this level of liquid filling is satisfied. However, when it is satisfied (at M) the transition to L' rapidly ensues, as for the upper branch. Branch BM therefore corresponds to a constant internal wetting of 75%.

If just before transition at V, which lies on the Kelvin branch and where the internal wetting is 43%, the mole fraction hydrogen is reduced further condensation will not occur till the Cohan equation is satisfied. This occurs at point N, and on further reducing y_B^o additional condensation rapidly ensues and the transition is obtained at M where 75% of the pore volume is liquid-filled. It may be expected that on increasing and decreasing the mole fraction y_B^o the points corresponding to the middle steady state will lie between the bounding branches VBM and VNM. This is indeed verified in Figure 4, where the majority of the middle branch data of Kim and Kim (1981a) lie between these two extremes.

Thus, we see that the data of Kim and Kim (1981a) can be explained on the basis of hysteresis effects related to the Kelvin and Cohan equations. In particular, the middle steady state corresponds to that for partial internal wetting of the micropores. This differs with one of their speculations that, since two pellets were used, one was in the lower micropore-liquid-filled state, while the other was in the upper vapor-filled state. Clearly, this speculation cannot explain any of the transitions from one branch to another. For example, the absence of the lower branch above a value of y_B^o of 0.125 and existence of a single branch above a value of y_B^o of 0.3 in Figure 4 would then imply that starting with a lower value of y_B^o, when micropores of both the pellets are filled with liquid (branch $L'L$ in Figure 4), if y_B^o is increased, at point L ($y_B^o = 0.125$) only one of the pellets would always undergo a transition to the completely vapor-filled state and the other would continue to be filled with liquid, until a value of y_B^o of 0.3 (point V, Figure 4) when the remaining pellet would also undergo a transition to the vapor-filled state. For this to be a reality, as dictated by capillary thermodynamics and indicated in Figure 3, the two pellets must be at considerably different temperatures and for uniform composition in a differential reactor such as the one used, this may be possible only when each of the pellets is exposed to entirely different heat transfer conditions (e.g., arrangement of packings). However, considering the reproducibility of the data on unpacking and repacking of the bed reported by Kim and Kim (1981a), this speculation for explaining the existence of the middle branch appears to be highly unlikely. The current model, on the other hand, offers a satisfactory interpretation of the data and all transitions, which were previously unexplained.

We thus see from the above the complexity of the steady-state behavior, occurring due to capillary condensation and evaporation effects, when condensables are involved in reaction. In particular, the uncertainty in the partial micropore wetting, middle steady state, being caused by the hysteresis between the Kelvin and Cohan limits is of great interest and can have important consequences in the operation of trickle-bed reactors. This hysteresis is directly evident from counter-clockwise hysteresis loop $EE''FF''E$ in Figure 5 which shows the changes in effectiveness factor with temperature at fixed bulk composition. Such changes can be induced by cycling some variables such as flow rate (which affects the heat transfer coefficient) so that history effects play a crucial role. While the impact may not be so severe in this case, as seen from the narrow band of effectiveness between branches VNM and VBM in Figure 4, it may be much more important for other more complex systems with a larger band.

Kim and Kim (1981a) have also provided hysteresis for another similar, but higher-activity, catalyst for which $q = 0.36$. Figure 6 shows the calculated and experimental effectiveness factor variation with y_B^o for this catalyst. The parameters are identical to those in Table 3, with ϕ_o taken as 28.41 because of the higher value of q. As before, good agreement is seen, with all the transitions satisfactorily predicted. Figures 7 and 8 show the predicted steady-state temperature—y_B^o plots cor-

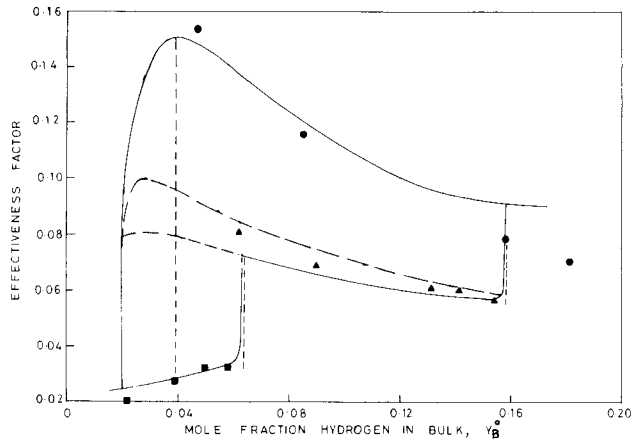

Figure 6. Model predictions vs. experimental data of Kim and Kim for effectiveness factor hysteresis with variation in bulk mole fraction hydrogen.

For medium-activity catalyst ($q = 0.36$) at $T_o = 295$ K.

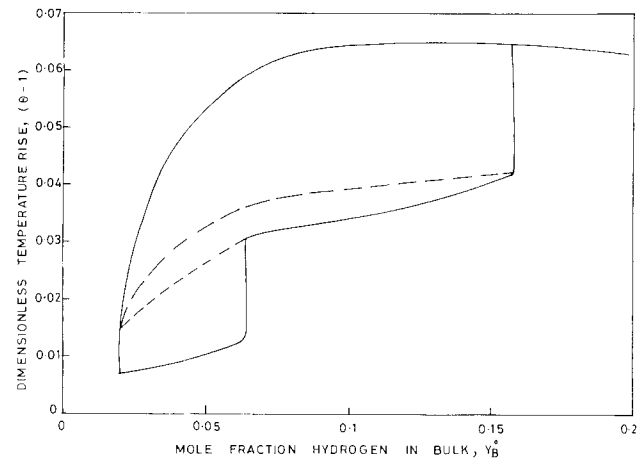

Figure 8. Temperature-composition hysteresis for catalyst with activity $q = 0.36$.

responding to Figures 4 and 6, indicating the jumps in temperature at the transitions. Such jumps have been reported by Hanika et al. (1976) in their studies of cyclohexene hydrogenation in trickle beds.

In performing the calculations for Figures 4–8, the unknown parameter β, related to the change in tortuosity with liquid filling (c.f. Eq. 13) was taken to be 1.24 and the tortuosity of the vapor-filled catalyst, τv, was taken as 4.0. The values were chosen for satisfactory matching with the data of the upper and lower branches in Figures 4 and 6. In addition, the parameter ψ was also obtained at each composition for matching of all the branches simultaneously. Figure 9 shows the estimated variation in ψ with bulk mole fraction y_B^o for the two catalysts. In addition to the rate data reported by Kim and Kim (1981a), they also measured actual catalyst temperatures and rates for another similar high-activity ($q = 1$) catalyst, for which the data were later provided by Kim (1989). From the latter data, the heat transfer coefficient, and hence ψ, could be directly estimated for each composition independent of the present model. Figure 9 shows the variation in ψ with y_B^o for this case superimposed with those estimated earlier for the other catalysts. The values lie within about 20%, well within the range of variations reported by Kim and Kim (1981a,b). Also superimposed is the correlation used by Kim and Kim which is seen to predict considerably higher values of ψ.

An assumption in the interpretation of the data of Kim and Kim is that the external mass transfer resistance is not significant. To verify this, the well known result (Froment and Bischoff, 1979)

$$y_B^o - y_B(1) = \frac{j_h C_P M P_{fB} T_o}{j_d(-\Delta H) P_T}\left[\frac{Sc_B}{Pr}\right]^{2/3}(\theta - 1)$$

was used along with the analogy $j_h = j_d$. The calculations for components A and B showed that indeed over the most of the range of compositions covered in Figures 4 and 6 the assumption was valid, although at the highest value of y_B^o of about 0.36, in Figure 4a 15% drop in the mole fraction of A (cyclohexene) in the external boundary layer was calculated. At lower values of y_B^o, this drop was lower and the assumption of negligible external resistance was satisfied even better. This observation is consistent with the fits of Figures 4 and 6 showing the tendency of the experimental values of effectiveness at

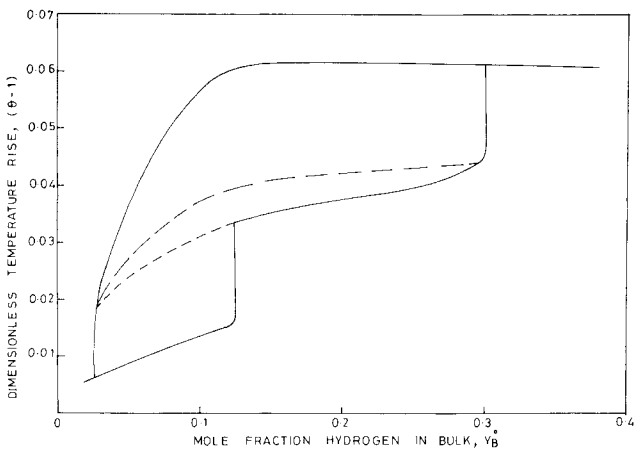

Figure 7. Temperature-composition hysteresis for catalyst with activity $q = 0.23$.

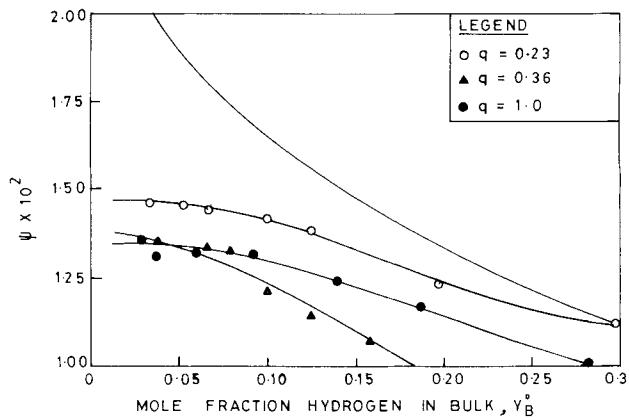

Figure 9. Estimated variation in ψ with bulk mole fraction y_B^o for different catalysts.

the upper and middle branches to be slightly below the predictions at the higher values of y_B^o. This would seem to be due to the increasing importance of the external mass transfer resistance with increasing value of y_B^o. It is also for this reason that the high-activity catalyst data (for which $q = 1$) provided by Kim (1989) were not quantitatively compared with the predictions of the present model, as the data cover the range of y_B^o up to 0.9 so that over most of the points the external mass transfer resistance is significant and cannot be neglected. Qualitatively, however, calculations did indicate that the middle steady state of partial micropore wetting in Figures 4 and 6 was not present for this catalyst, consistent with the reports of Kim and Kim.

A factor worth noting is that while the literature is replete with the models of pore structure the one used here for the micropores is the simplest one of these, being based on an intersecting cylindrical capillary network. More complex models could have been considered but their choice is generally motivated by the method of generation of the internal structure. Thus, for example, for the interparticle pore space a model based on converging-diverging channels often suggests itself as a possible alternative. However, for the intragrain micropores, in which the partial internal wetting considered here occurs, there is as yet no firm physical justification for preferring a more complex model and hence recourse has been taken to the cylindrical capillary one. The refinement of considering other more complex models in analyzing partial internal wetting is therefore an open problem, but *a priori* it is not clear if the conclusions would be different substantially.

Conclusion

In this work, the unusual behavior shown by catalyst particles exposed to condensable vapor has been investigated. The process of condensation and evaporation in porous media do not necessarily take place as exact reverses of each other, so that hysteresis effects arise in a catalyst particle leading to uncertainty in predicting the extent of internal wetting and associated reaction rate. The intriguing and complex behavior observed experimentally by Kim and Kim (1981a) in a catalyst pellet exposed to condensable vapor could be predicted and satisfactorily explained using a mathematical model incorporating established capillary condensation theory. The effective diffusivity, on which the observed reaction rate depends so strongly, is influenced by the extent of internal wetting which itself is sensitive to thermal effects and cannot be ascertained unless the thermal history of the pellet is known. For a given process condition, however, the Cohan and Kelvin equations can be used to obtain upper and lower limits of the extent of internal wetting, and hence the two extreme values of effectiveness factor for a given bulk condition can be determined.

Notation

a,b,c = stoichiometric factors
C_P = heat capacity
C_T^o = total gas-phase concentration at bulk conditions
$d_{AB} = D_{AC}^o/D_{AB}^o$
$d_{AI} = D_{AC}^o/D_{AI}^o$
$d_{AK} = D_{AC}^o/D_{K,A}^o(\mu_i)$
$d_{BC} = D_{AC}^o/D_{BC}^o$
$d_{BI} = D_{AC}^o/D_{BI}^o$
$d_{BK} = D_{AC}^o/D_{K,B}^o(\mu_i)$
$d_{CI} = D_{AC}^o/D_{CI}^o$
$d_{CK} = D_{AC}^o/D_{K,C}^o(\mu_i)$
D_{ij} = binary diffusivity
D_{ij}^o = D_{ij} at bulk temperature
D_{Am}^* = see Eq. 16
D_{Bm}^* = see Eq. 17
D_{Cm}^* = see Eq. 18
D_{eA}^* = see Eq. 10
D_{eB}^* = see Eq. 11
D_{eC}^* = see Eq. 12
$D_{K,i}^o$ = Knudsen diffusivity for component i at bulk temperature
E = effectiveness factor
$f(\rho)$ = see Eq. 15
h = external heat transfer coefficient
$h_i = \bar{v}_i/\bar{v}_A$
ΔH = heat of reaction
ΔH_i^* = $\Delta H_i/R_gT_o$, dimensionless enthalpy of vaporization of pure i
j_d = mass transfer Colburn j factor
j_h = heat transfer Colburn j factor
k = reaction rate constant
k_o = value of kP_T^m for the vapor-filled catalyst at 295 K
K_{Pe} = effective permeability
m = order of reaction
m_o = order of vapor-phase reaction at bulk temperature
M = mean molecular weight
N_A = molar flux of A
N_T = total molar flux
P_f = film pressure factor
P_i^o = vapor pressure of component i at temperature T
$P_i^{o*} = P_i^o/P_T$
$P_{io}^* = P_i^o(T_o)/P_T$
Pr = Prandtl number
P_T = total pressure
$\Delta P_{\max}^*$ = see Eq. A4
q = constant for adjusting the activity
r = pore radius
r_1, r_2 = principal radii of curvature
r_c = critical pore radius
r_m = mean radius of curvature of the meniscus
r_M = mean macropore radius
R = radial position
$\hat{R}_A$ = see Eq. 4
R_c = radial position at which $y_A = 0$
R_o = 3 (V/S), equivalent sphere radius
R_g = universal gas constant
S = external surface area of the pellet
Sc = Schmidt number
T = temperature
T_o = bulk temperature
$\bar{v}_i$ = partial molar volume of component i
V = pellet volume
y_i = mole fraction of component i
y_i^o = bulk mole fraction of component i

Greek letters

$\alpha = 2\sigma\bar{v}_A/\mu_i R_g T_o$
β = see Eq. 13
δ_A = see Eq. A2
ϵ = total porosity
ϵ_L = percent liquid filling of the pore structure
ϵ_M = macroporosity
$\eta = R/R_o$
$\eta_c = R_c/R_o$
μ = viscosity
μ_i = mean micropore radius
$\phi_o = R_o\left[\dfrac{qk_o\tau_v}{\epsilon D_{AC}^o C_T^o}\right]^{1/2}$
ϕ = see Eq. 9
$\psi = (-\Delta H)D_{AC}^o C_T^o \epsilon/\tau_v R_o h T_o$
$\rho = r/\mu_i$

ρ_c = r_c/μ_i
τ = tortuosity factor
τ_v = τ for vapor-filled catalyst
τ^* = see Eq. 13
θ = T/T_o
$\hat{\theta}$, θ_c = contact angle
σ = surface tension

Literature Cited

Bhatia, S. K., "Steady-State Multiplicity and Partial Internal Wetting of Catalyst Particles," *AIChE J.*, **34**, 969 (1988).

Bhatia, S. K., "Partial Internal Wetting of Catalyst Particles with a Distribution of Pore Size," *AIChE J.*, **35**, 1337 (1989).

Eigenberger, G., and V. Wegerle, "Runaway in an Industrial Hydrogenation Reactor," *ACS Symp. Ser.*, **196**, 133 (1982).

Everett, D. H., and J. M. Haynes, "Model Studies of Capillary Condensation: 1. Cylindrical Pore Model with Zero Contact Angle," *J. Colloid Interface Sci.*, **38**, 125 (1972).

Finlayson, B., *The Method of Weighted Residuals and Variational Principles*, Academic Press, New York (1972).

Froment, G. F., and K. B. Bischoff, *Chemical Reactor Analysis and Design*, Wiley, New York (1979).

Germain, A. H., A. G. Lefebvre, and G. A. L'Homme, "Experimental Study of a Catalytic Trickle-Bed Reactor," *Adv. Chem. Ser.*, **133**, 164 (1974).

Gregg, S. J., and K. S. W. Sing, *Adsorption, Surface Area and Porosity*, Academic Press, New York (1967).

Hanika, J., K. Sporka, V. Ruzicka, and J. Krausova, "Qualitative Observations of Heat and Mass Transfer Effects on the Behavior of a Trickle-Bed Reactor," *Chem. Eng. Commun.*, **2**, 19 (1975).

Hanika, J., K. Sporka, V. Ruzicka, and J. Hrstka, "Measurements of Axial Temperature Profiles in an Adiabatic Trickle-Bed Reactor," *Chem. Eng. J.*, **12**, 193 (1976).

Harold, M. P., "Steady-State Behavior of the Nonisothermal Partially Wetted and Filled Catalyst," *Chem. Eng. Sci.*, **43**, 3197 (1988a).

Harold, M. P., "Partially Wetted Catalyst Performance in the Consecutive Parallel Network," *AIChE J.*, **34**, 980 (1988b).

Herskowitz, M., "Wetting Efficiency in Trickle-Bed Reactors. The Overall Effectiveness Factor of Partially Wetted Catalyst Particles," *Chem. Eng. Sci.*, **36**, 1665 (1981a).

Herskowitz, M., "Wetting Efficiency in Trickle-Bed Reactors: Its Effect on Reactor Performance," *Chem. Eng. J.*, **22**, 167 (1981b).

Kim, D. H., and Y. G. Kim, "An Experimental Study of Multiple Steady-States in a Porous Catalyst Due to Phase Transition," *J. Chem. Eng. Japan*, **14**, 311 (1981a).

Kim, D. H., and Y. G. Kim, "Simulation of Multiple Steady-States in a Porous Catalyst Due to Phase Transition," *J. Chem. Eng. Japan*, **14**, 318 (1981b).

Kim, D. H., personal communication (1989).

Kirpatrick, S., "Classical Transport in Disordered Media: Scaling and Effective-Medium Theories," *Phys. Rev. Lett.*, **27**, 1722 (1971).

Kirpatrick, S., "Percolation and Conduction," *Rev. Mod. Phys.*, **45**, 574 (1973).

Lee, T. J., MSc Thesis, Korea Advanced Institute of Science, Seoul, Korea (1980).

Madon, R. J., J. P. O'Conell, and M. Boudart, "Catalytic Hydrogenation of Cyclohexene: II. Liquid Phase Reaction on Supported Platinum in a Gradientless Slurry Reactor," *AIChE J.*, **24**, 904 (1978).

Martinez, O. M., G. F. Barreto, and N. O. Lemcoff, "Effectiveness Factor of a Catalyst Pellet in a Trickle-Bed Reactor—Limiting Reactant in the Gas Phase," *Chem. Eng. Sci.*, **36**, 901 (1981).

Mills, P. L., and M. P. Dudukovic, "Application of the Method of Weighted Residuals to Mixed Boundary Value Problems: Dual Series Relations," *Chem. Eng. Sci.*, **35**, 1557 (1980).

Mills, P. L., and M. P. Dudukovic, "Integral Equation Solution for the Effectiveness Factor of the Partially Wetted Catalysts," *Ind. Eng. Chem. Fund.*, **21**, 90 (1982).

Mohanty, K. K., J. M. Ottino, and H. T. Davis, "Reaction and Transport in Disordered Composite Media: Introduction of Percolation Concepts," *Chem. Eng. Sci.*, **37**, 905 (1982).

Ramchandran, P. A., and J. M. Smith, "Effectiveness Factors in Trickle-Bed Reactors," *AIChE J.*, **25**, 538 (1979).

Sakornwimon, W., and N. D. Sylvester, "Effectiveness Factors for Partially Wetted Catalysts in Trickle-Bed Reactors," *Ind. Eng. Chem. Process. Des. Dev.*, **21**, 16 (1982).

Satterfield, C. N., and F. Ozel, "Direct Solid-Catalyzed Reaction of a Vapor in an Apparently Completely Wetted Trickle-Bed Reactor," *AIChE J.*, **19**, 1259 (1973).

Satterfield, C. N., and P. F. Way, "The Role of the Liquid Phase in the Performance of a Trickle-Bed Reactor," *AIChE J.*, **18**, 305 (1972).

Sedricks, W., and C. N. Kenney, "Partial Wetting in Trickle-Bed Reactors—The Reduction of Crotonaldehyde Over a Palladium Catalyst," *Chem. Eng. Sci.*, **28**, 559 (1973).

Segal, E., R. J. Madon, and M. Boudart, "Catalytic Hydrogenation of Cyclohexene: 1. Vapor-Phase Reaction on Supported Platinum," *J. Catal.*, **52**, 45 (1978).

Tan, C. S., "Effectiveness Factors of *n*th Order Reactions for Incomplete Wetting of Particles in Trickle-Bed Reactors," *Chem. Eng. Sci.*, **43**, 1281 (1988).

Tukac, V., I. Mazzarrino, G. Baldi, A. Gianetto, S. Sicardi, and V. Specchia, "Conversion Rates in a Laboratory Trickle-Bed Reactor During the Oxidation of Ethanol," *Chem. Eng. Sci.*, **41**, 17 (1986).

Wicke, E., and A. Bartsch, "Percolation and Blocking in Supported Liquid-Phase Catalysts: Styrene Catalyst as a Particular Case," *Ind. Eng. Chem. Res.*, **29**, 994 (1990).

Yentekakis, I. V., and C. G. Vayenas, "Effectiveness Factors for Reactions Between Volatile and Nonvolatile Components in Partially Wetted Catalysts," *Chem. Eng. Sci.*, **42**, 1323 (1987).

Appendix: Validity of the Isobaric Assumption

Since we have assumed isobaric conditions in the interior of the pellet for the experimental conditions of Kim and Kim (1981a), we theoretically justify here the validity of this assumption.

To this end, consider the reaction $aA + bB \rightarrow cC$ where A, B and C in this case represent cyclohexene, hydrogen and cyclohexane, respectively. The total molar flux $N_T(R)$ and molar flux of component A, $N_A(R)$, at any position R, are related by:

$$N_T(R) = \delta_A N_A(R) \tag{A1}$$

where

$$\delta_A = 1 + \frac{b}{a} - \frac{c}{a} \tag{A2}$$

To estimate the pressure drop inside the pellet we express the fluxes and viscous species in terms of the respective constitutive equations and obtain the upper bound for the pressure gradient:

$$\frac{K_{Pe}}{\mu}\frac{dP}{dR} = \delta_A D_{eA}\frac{dy_A}{dR} \tag{A3}$$

where, as stated earlier, the effective diffusivity D_{eA} includes any bulk flow arising due to reaction. Considering K_{Pe} and D_{eA} to be constant, Eq. A3 can be integrated to obtain the maximum pressure drop $\Delta P^*_{\max}$ (dimensionless) corresponding to the complete consumption of A in the pellet:

$$\Delta P^*_{\max} = \frac{D_{eA}\mu\delta_A y^o_A}{K_{Pe}P_T} \tag{A4}$$

We evaluate the typical maximum pressure drop by considering point V on the partial wetting (middle) branch (c.f. Figure 4).

Since the dominant contribution to the permeability will be from the macropores, we evaluate $K_{P\theta}$ as:

$$K_{Pe}=\frac{r_M^2\epsilon_M}{24} \tag{A5}$$

where r_M is the mean macropore radius, and ϵ_M the macroporosity, in which the tortuosity factor for bulk flow is taken to be equal to 3. At point V the computations yielded $D_{eA}=2.76\times10^{-8}$ m^2/s (based on Eq. 10) and, using the data provided in Tables 1-3 along with the values $\mu=10^{-5}$ Pa·s, $P_T=101$ kPa, we obtain $\Delta P^*_{\max}=0.0036$, a relatively small number.

To establish the validity of the assumption of isobaric conditions, however, it is necessary also to evaluate the effect of the pressure variation on the estimated value of r_c. For this purpose, we consider the radial position of minimum pressure. At this location, where the component A (cyclohexene) is completely consumed, we use the Kelvin equation to obtain

$$\frac{P_T(1-\Delta P^*_{\max})y_c}{P^o_C(T)}=\exp\left[-\frac{2\sigma\bar{v}_c}{r_cR_gT}\right] \tag{A6}$$

At the point V on the partial wetting branch, computations yielded $y_c=0.1$ and $T=308$ K [corresponding to dimensionless temperature rise $(\theta-1)=0.044$]. Using Eq. 22 and the parameters listed in Table 3, we obtain

$$\frac{r_c(\Delta P^*_{\max}=0.0)}{r_c(\Delta P^*_{\max}=0.0036)}=1.006$$

Similar calculations for any point on branch MBV (c.f. Figure 4) show the relative insensitivity of the estimated value of r_c to the pressure variation.

Thus, our assumption of isobaric conditions is justifiable. This analysis, however, is specific to this particular investigation. For other experimental conditions or systems, r_c can be very sensitive to even small pressure gradients, and depending on pore size distribution this may significantly affect the results.

Manuscript received Apr. 30, 1990, and revision received Jan. 29, 1991.